arXiv:nucl-th/0101025v1 13 Jan 2001

Presented in October 2000 at the 6th International Workshop on
Relativistic Aspects of Nuclear Physics
Tabatinga, Sao Paulo, Brazil

THE STRANGE QUARK-GLUON PLASMA

JOHANN RAFELSKI AND GIORGIO TORRIERI
Department of Physics, University of Arizona, Tucson, AZ, 85721

JEAN LETESSIER
Laboratoire de Physique Théorique et Hautes Energies
Université Paris 7, 2 place Jussieu, F–75251 Cedex 05

Strangeness flavor has turned out to be a very effective diagnostic tool of relativistic heavy ion physics. The absolute yield provides information about conditions arising in first instants of the interaction. Strange hadrons are abundant allowing a precise study of the chemical freeze-out conditions in the dense matter fireball. The thermal and chemical freeze-out universality seen in strange hadrons confirms sudden hadronization as the breakup mechanism. A plausible cause of sudden fireball breakup is the mechanical instability arising when a quark-gluon plasma phase supercools deeply in its adiabatic expansion. Applying these ideas, we interpret CERN-SPS and the first results on hadronic particle ratios obtained at RHIC.

1 Introduction

It is believed today that a new state of matter has been formed in relativistic nuclear collisions at CERN. The question is if this is the hot quark matter (quark-gluon plasma) state of matter, which has been for 30 years a predicted new form of elementary matter: as early as 1970, the development of the quark model lead to a first consideration of quark matter stellar structure. [1]

These ideas were deepened by the development of the quantum many body theory of quark matter, [2,3] which lead on to the formal recognition within the framework of asymptotically free quantum-chromodynamics (QCD) that a very high temperature perturbative quark matter state must exist. [4] Other reasoning based on a study of the 'boiling state' of dense hadron gas within the scheme of Hagedorn's statistical bootstrap of hadronic matter has independently lead from a different direction to the consideration of the transition to a hadron substructure phase. [5] Considering the present day lattice-QCD numerical simulations, [6] we understand today quite well the properties of the baryon number free quark-gluon plasma (QGP), as we today call hot quark matter

However, it is still common to study ad-hoc ideas about new phases of fundamental matter. This is a natural approach considering the history of nuclear physics which developed without fundamental knowledge about the quark/QCD nature of nuclear interactions. Nuclear physics advanced by the

development of models, and this tradition remains strong. In fact there was little initial interest in quarks, gluons, and QCD among nuclear physisists. The first of the series of formative workshops in the field of relativistic heavy ion collisions, the "Bear Mountain" meeting in November 1974 had not a single mention of quarks, let alone of quark matter. At the time ultra dense nuclei, multi-hyperon nuclear states, and "pion condensates", were all considered as the discovery potential of these new and coming tools of nuclear physics research.

As the ideas about QGP formation in high energy nuclear collision matured, an unexpected challenge emerged 20 years ago: how can the locally deconfined state which exists a mere 10^{-22}s be distinguished from the gas of confined hadrons? This is also a question of principle, considering that both quark and hadron pictures of the reaction could be equivalent, for it has been argued that a quark-gluon based description is merely a change of Hilbert space expansion basis, if the rules of quantum mechanics with pure states are considered. This view contradicts the intuition, and about everybody in our field has come to believe that QGP phase is observable, since the quantum solution decoheres, even if the argument is being made with a lot of hand waving.

In the Galilean tradition, such a difficult question about existence and observability of a new phase of elementary matter, the QGP, must be settled by an experiment. This requires that a probe of QGP operational on the collision time scale of $5{\cdot}10^{-23}$ s is developed, which is sensitive to the local color charge deconfinement, and that it depends on the gluon degree of freedom, which is the characteristic new ingredient of the quark matter phase.

One of us (JR) proposed strangeness as the signature of QGP noticing more than 20 years ago that when color bonds are broken, the chemically equilibrated deconfined state has an unusually high number of strange quark pairs. [7] A study of the dynamics of strangeness (chemical) equilibration process has shown that only the gluon component in the QGP is capable to produce strangeness rapidly [8], allowing the formation of (nearly) chemically equilibrated dense phase of deconfined, hot, strangeness-rich quark matter in relativistic nuclear collisions. Therefore, strangeness enhancement is related directly to the presence of gluons in QGP.

The high density of strangeness available in the fireball favors during hadronization the formation of multi-strange hadrons, [9,10] which are produced quite rarely if only individual hadrons collide. [11,12] A large enhancement of multi strange (anti)baryons has been continuously advanced and defended by one of us (JR) as a characteristic signature of the QGP over the past 20 years. A systematic enhancement has been now reported, rising with strangeness

content. [13] Here the enhancement of strange antibaryons is reported with a base being the expectation derived from the scaled nucleon-nucleon and nucleon-nucleus reactions.

These experimental results are consistent with particle production occurring from a strangeness dense source in which the strange quarks are already made, are freely moving around and are readily available. This is by definition, the deconfined state we refer to as the quark-gluon plasma. We are not aware of a consistent interpretation of the rich and diverse experimental results not using QGP formation. It is important here to remember that since there are many results on strange hadron production, any alternative description has to be tested on all data available.

We think that strangeness enhancement has turned out to be a very practical signature of quark-gluon plasma physics. This report summarizes our work of past 18 months in this area – for further details the reader may consult our recent articles. [14,15,16,17] In the following section 2 we will describe our most recent advances in the study of properties of QGP at time of its formation and its sudden breakup. [15] The initial conditions are determining the overall strangeness yield. We use the properties of QGP at sudden breakup in the following section 3, testing the consistency of the chemical freeze-out condition with the properties of the QGP. [14] Recently, [16] we have been able to understand the mechanism of sudden QGP hadronization in terms of a mechanical instability arising within a supercooled and rapidly expanding fireball, as we will discuss in section 4.

An important experimental observation pointing to sudden QGP breakup is that strange baryons and antibaryons have very similar $m_\perp$-spectra [18] and are thus produced by the same mechanism. [19] Moreover, as we will show in section 5, these spectra imply that the thermal freeze-out of these rarely produced particles occurs together with the chemical (abundance) freeze-out. [17] This occurs for all collision centralities measured by experiment WA97.

In recent months first strangeness results have been obtained at RHIC. Our analysis effort regarding these results has just begun. Some of our RHIC predictions [20,21] can already be compared with experiment, and we will show in section 6 to be in agreement with our picture of how strangeness and QGP evolves at RHIC.

2 QGP fireball

2.1 Formulation of the QGP model

Using the latest lattice-QCD results, we have been able to better model the properties of the QGP, [15] compared to our earlier considerations. [22] The key ingredients of our current approach are:

1. We relate the QCD scale to the temperature $T = 1/\beta$, we use for the scale the Matsubara frequency [23] (μ without a subscript is *not* a chemical potential, it is the QCD scale):

$$\mu = 2\pi\beta^{-1}\sqrt{1 + \frac{1}{\pi^2}\ln^2\lambda_{\rm q}} = 2\sqrt{(\pi T)^2 + \mu_{\rm q}^2}\,. \tag{1}$$

   This extension to finite chemical potential $\mu_{\rm q}$, or equivalently quark fugacity $\lambda_{\rm q} = \exp\mu_{\rm q}/T$, is motivated by the form of plasma frequency entering the computation of the vacuum polarization function. [24]

2. We obtain the interacting strength $\alpha_s(\mu)$ integrating numerically the renormalization group equations

$$\mu\frac{\partial\alpha_s}{\partial\mu} = -b_0\alpha_s^2 - b_1\alpha_s^3 + \ldots \equiv \beta_2^{\rm pert}\,. \tag{2}$$

   $\beta_2^{\rm pert}$ is the beta-function of the renormalization group in two loop approximation, and

$$b_0 = \frac{11 - 2n_{\rm f}/3}{2\pi}\,, \quad b_1 = \frac{51 - 19n_{\rm f}/3}{4\pi^2}\,.$$

   $\beta_2^{\rm pert}$ does not depend on the renormalization scheme, and solutions of Eq. (2) differ from higher order renormalization scheme dependent results by less than the error introduced by the experimental uncertainty in the measured value of $\alpha_s(\mu = M_Z) = 0.118 + 0.001 - 0.0016$.

3. We introduce, in the domain of freely mobile quarks and gluons, a finite vacuum energy density:

$$\mathcal{B} = 0.19\,\frac{\rm GeV}{\rm fm^3}\,.$$

   This also implies, by virtue of relativistic invariance, that there must be a (negative) associated pressure acting on the surface of this volume, aiming to reduce the size of the deconfined region. These two properties of the vacuum follow consistently from the vacuum partition function:

$$\ln\mathcal{Z}_{\rm vac} \equiv -\mathcal{B}V\beta\,. \tag{3}$$

4. The partition function of the quark-gluon liquid comprises interacting gluons, $n_{\rm q}$ flavors of light quarks, [25] and the vacuum $\mathcal{B}$-term. We incorporate further the strange quarks by assuming that their mass in effect reduces their effective number $n_{\rm s} < 1$:

$$\begin{aligned}\frac{T}{V}\ln \mathcal{Z}_{QGP} \equiv P_{\rm QGP} \ &= -\mathcal{B} + \frac{8}{45\pi^2}c_1(\pi T)^4 \\ &+\frac{n_{\rm q}}{15\pi^2}\left[\frac{7}{4}c_2(\pi T)^4 + \frac{15}{2}c_3\left(\mu_{\rm q}^2(\pi T)^2 + \frac{1}{2}\mu_{\rm q}^4\right)\right] \\ &+\frac{n_{\rm s}}{15\pi^2}\left[\frac{7}{4}c_2(\pi T)^4 + \frac{15}{2}c_3\left(\mu_{\rm s}^2(\pi T)^2 + \frac{1}{2}\mu_{\rm s}^4\right)\right] \quad (4)\end{aligned}$$

where:

$$c_1 = 1 - \frac{15\alpha_s}{4\pi} + \cdots, \quad c_2 = 1 - \frac{50\alpha_s}{21\pi} + \cdots, \quad c_3 = 1 - \frac{2\alpha_s}{\pi} + \cdots . \quad (5)$$

2.2 Properties of QGP-liquid

We show properties of the quark-gluon liquid defined by Eq. 3 in a wider range of parameters at fixed entropy per baryon S/B, in the range $S/B = 10$–60 in step of 5 units. In the top panel in figure 1, we show baryo-chemical potential μ_b, in middle panel baryon density n/n_0, here $n_0 = 0.16/\mathrm{fm}^3$, and bottom left the energy per baryon E/B. In top and middle panel the low entropy results are top-left in figure, in bottom panel bottom left. The highlighted curve, in figure 1, is for the value $S/B = 42.5$, applicable to the 158 AGeV Pb–Pb collisions. The dotted line, at the minimum of $E/B|_{S/B}$, is where the vacuum and quark-gluon gas pressure balance.

Little entropy is produced during the nearly adiabatic evolution of the QGP fireball. [26] Thus the lines in the lower panel of figure 1 characterize the approximate trajectory in time of the fireball. After initial drop in energy per baryon due to transfer of energy to accelerating expansion of the fireball, during the deep supercooling process, the motion is slowed and thus energy per baryon increases. The thick line is our expectation for the fireball made in Pb–Pb interactions at the projectile energy 158A GeV. The cross shows the result of chemical freeze-out analysis presented in next section 3. [14]

We also have compared the chemical freeze-out conditions with the phase transition properties. The hadron gas behavior is obtained evaluating and summing the contributions of all known hadronic resonances considered to be point particles. The thin solid line in the $T, \mu_{\rm b}$ plane in figure 2 shows where the pressure of the quark-gluon liquid equals the equilibrated hadron gas pressure. When we allow for finite volume of hadrons, [27] we find that

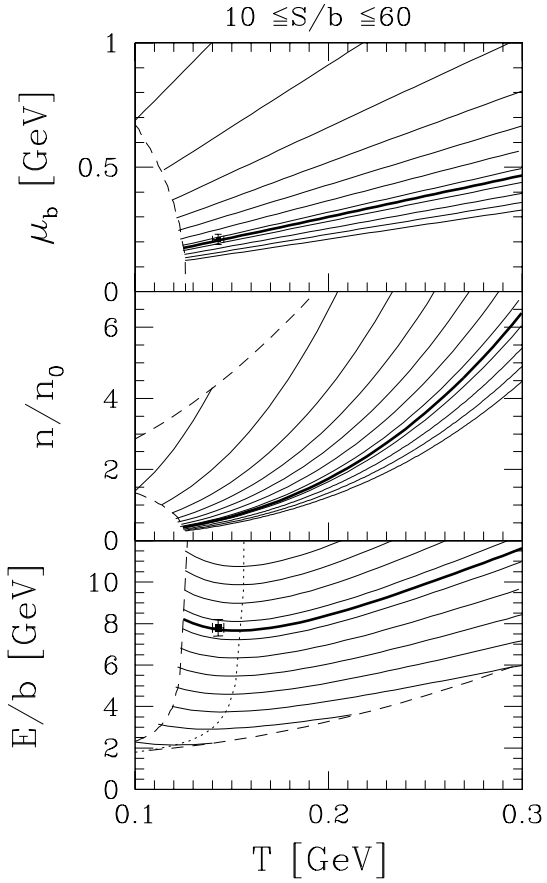

Figure 1. From top to bottom: μ_b, n/n_0 and E/B; lines shown correspond to fixed entropy per baryon $S/B = 10$ to 60 by step of 5 (left to right). Thick solid lines: result for $S/B = 42.5$. Limits: energy density $\varepsilon_{q,g} = 0.5\,\mathrm{GeV/fm^3}$ and baryo-chemical potential $\mu_b = 1\,\mathrm{GeV}$. The experimental points denote chemical freeze-out analysis result. [14]

the hadron pressure is slightly reduced, leading to some (5 MeV) reduction in the equilibrium transition temperature, as is shown by the dashed line in figure 2 . For vanishing baryo-chemical potential, we note in figure 2 that the equilibrium phase transition temperature is $T_{\rm pt} \simeq 172\,\mathrm{MeV}$, and when finite hadron size is allowed, $T_{\rm fp} \simeq 166\,\mathrm{MeV}$, The scale in temperature we discuss is result of comparison with lattice gauge results. Within the lattice calculations [6], it arises from the comparison with the string tension.

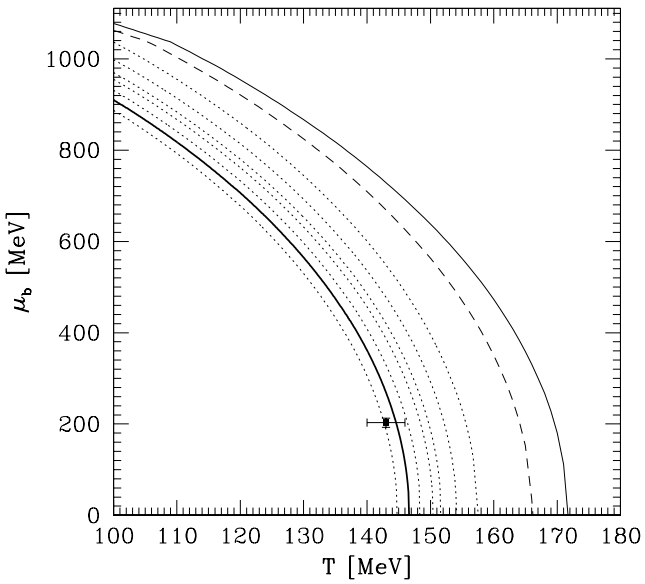

Figure 2. Thin solid and dashed lines: equilibrium phase transition from hadron gas to QGP liquid without and with excluded volume correction, respectively. Dotted: breakup condition at shape parameter $\kappa = 0.6$, for expansion velocity $v_c^2 = 0, 1/10, 1/6, 1/5, 1/4$ and $1/3$, and thick line for $v_c = 0.54$. The experimental point denotes chemical non-equilibrium freeze-out analysis result. [14]

The dotted lines, in figure 2, show where the flowing QGP liquid has a pressure which balances the vacuum pressure, and thus these lines correspond to sudden break up at a velocity for (from right to left) $v_c^2 = 0, 1/10, 1/6, 1/5, 1/4$ and $1/3$, see section 4, specifically the dotted lines in figure 2 correspond to the condition Eq. (9) using the shape parameter $\kappa = 0.6$, Eq. (12). The last dotted line corresponds thus to an expansion flow with the velocity of sound of relativistic noninteracting massless gas. The thick solid line corresponds to an expansion with $v_c = 0.54$. The hadron analysis result is also shown as presented in section 3. [14] Comparing in figure 2 thin solid/dashed with the thick line, we recognize the deep supercooling as required for the explosive fireball disintegration. The super-cooled zero pressure $P = 0$ baryonfree QGP temperature is at $T_{sc} = 157\,\mathrm{MeV}$, (see the intercept of the first dashed line to the right in figure 2) and an expanding fireball can deeply super-cool to $T_{dsc} \simeq 147\,\mathrm{MeV}$ (see the intercept of thick solid line) before the mechanical instability occurs.

2.3 Initial conditions in QGP formation

The formation of the QGP occurs well before chemical equilibration of quarks. We model this situation varying n_f. For $n_f = 1$ we show, in figure 3, lines of fixed energy per baryon E/B =3, 4, 5, 6, 8, 10, 20, 50 and 100 GeV, The horizontal solid line is where the equilibrated hadronic gas phase has the same pressure as QGP-liquid with semi-equilibrated quark abundance. The free energy of the QGP liquid must be lower (pressure higher) in order for hadrons to dissolve into the plasma phase. The dotted lines in figure 3, from bottom to top, show where the pressure of the semi-equilibrated QGP phase is equal to $\eta = 20\%, 40\%, 60\%, 80\%$ and 100%, η being the 'stopping' fraction of the dynamical collisional pressure [22]:

$$P_{\rm col} = \eta\rho_0 \frac{P_{\rm CM}^2}{E_{\rm CM}}\,. \tag{6}$$

The rationale to study, in figure 3, lines at fixed E/B is that, during the nuclear collision which lasts about $2R_N/\gamma_L 2c \simeq 13/18\,{\rm fm}/c$, where γ_L is the Lorentz factor between the lab and CM frame and R_N is the nuclear radius, parton collisions lead to a partial (assumed here to be 1/2) chemical equilibration of the hadron matter. At that time, the pressure exercised corresponds to collisional pressure $P_{\rm col}$. This stopping fraction, seen in the transverse energy produced, is about 40% for S–S collisions at 200A GeV and 60% for Pb–Pb collisions at 158A GeV. If the momentum-energy and baryon number stopping are similar, as we see in the experimental data, then the SPS collisions at 160–200A GeV are found in the highlighted area left of center of the figure. In the middle of upper boundary of this area, we would expect the beginning evolution of the thermal but not yet chemically equilibrated Pb–Pb fireball, and in the lower left corner of the S–S fireball. We note that the temperature reached in S–S case is seen to be about 25 MeV lower than in the Pb–Pb case. The lowest dotted line (20% stopping) nearly coincides with the non-equilibrium phase boundary (solid horizontal line, in figure 3) and thus we conclude that this is, for the condition $n_f = 1$, the lowest stopping that can lead to formation of a deconfined QGP phase. Such a low stopping would be encountered possibly in lighter than S–S collision systems or/and at large impact parameter interactions of larger nuclei.

The highlighted area, right of center of the figure 3, corresponds to the expected conditions in Pb–Pb collisions at 40A GeV. If we assume that the stopping here is near 80%, then the initial conditions for fireball evolution would be found towards the upper right corner of this highlighted area. We recognize that the higher stopping nearly completely compensates the effect of reduced available energy in the collision and indeed, we expect that we form

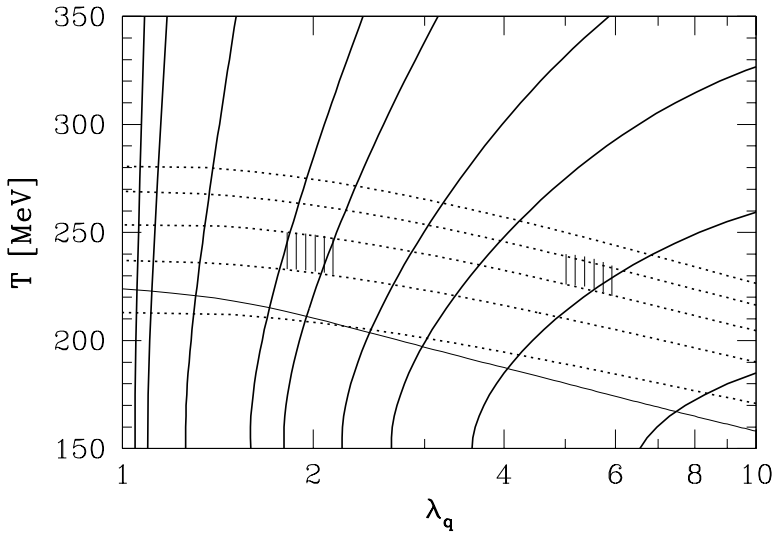

Figure 3. Contours of energy per baryon in QGP in the T–λ_q plane for $n_f = 1$: From right to left E/B=3, 4, 5, 6, 8, 10, 20, 50 and 100 GeV . Thin, nearly horizontal line: hadronic gas phase has the same pressure as the QGP-liquid with semi-equilibrated quark flavor. Dotted lines from bottom to top: pressure in QGP liquid equals $20\%, 40\%, 60\%, 80\%,$ and 100%, of the dynamical collisional pressure.

QGP also at these collision energies. It is important to realize that we are entering a domain of parameters, in particular λ_q, for which the extrapolation of the lattice results is not necessarily reliable, and thus our equations of state have increased systematic uncertainty.

3 Fermi-model data analysis

3.1 Properties of hadronic matter fireball

A full account of our prior analysis of the 158A GeV Pb–Pb collision system has appeared. [14] We briefly summarize the results that we require for the study of QGP properties at fireball breakup. In table 1, in upper section, we present the parameters T_f (the chemical freeze-out temperature), v_c (the

collective flow velocity at sudden breakup), λ_q (the light quark fugacity), λ_s (the strange quark fugacity), γ_q (the light quark phase space occupancy), γ_s (the strange quark phase space occupancy). These chemical properties are derived from analysis of all hadrons excluding Ω and $\overline{\Omega}$, which data points are not following the same systematic production pattern. These parameters characterize completely the physical properties of the produced hadrons, and these properties are shown in the bottom section of table 1.

In the heading of the table, the total error, χ^2 is shown, along with the number of data points N, parameters p and data point constraints r. The confidence level that is reached in our description is near or above 90%, depending on scenario considered. The scenarios we consider are seen in the columns of table 1: an unconstrained description of all data in the first column, constraint to exact strangeness conservation in the observed hadrons, second column. Since in both cases the parameter γ_q assumes value that maximizes the entropy and energy content in the pion gas, we assume this value in the so constrained third column.

We can now check the consistency between the statistical parameters (top panel of table 1) and the physical properties of the fireball (bottom panel of table 1) which are maintained in the process of hadronization. We note that the energy shown in this table, is the intrinsic energy in the flowing frame. The CM-laboratory energy includes the kinetic energy of the flow and thus is greater, to be obtained multiplying the result shown in table 1 by the Lorenz factor $\gamma = 1/\sqrt{1-v_c^2} = 1.19$. Thus the initial value of the energy per baryon that the system had before expansion started has been $E^0/B \simeq 9.3\,\mathrm{GeV}$.

3.2 Interpretation in terms of QGP

In the bottom panel in figure 1, we saw that the Temperature $T_f = 143 \pm 3\,\mathrm{MeV}$ and intrinsic (frame at rest) energy per baryon $E/B = 7.8\,\mathrm{GeV}$ where just at $S/B = 42.5$ seen table 1. Similarly, in the top panel, the baryo-chemical potential $\mu_b = 3T_f \ln \lambda_q = 204 \pm 10\,\mathrm{MeV}$ is as required for the consistency of QGP properties. The fireball hadron freeze-out and/or breakup condition is thus found well below the QGP to HG phase transition temperature. Both the specific energy and entropy content of the fireball are consistent with the statistical parameters T_f and μ_b according to our equations of state of the quark-gluon liquid. We can also evaluate the hadronic phase space energy density. We allow the excluded volume correction. [27] Considering that the point particle phase space energy density $\varepsilon_{pt} = 1.1\,\mathrm{GeV/fm^3}$, we obtain $\varepsilon_{HG} \simeq 0.4\,\mathrm{GeV/fm^3}$ at chemical freeze-out, using the value of $\mathcal{B} = 0.19\,\mathrm{GeV/fm^3}$. This energy density is neraly the same as one finds in QGP. Thus we see that

Table 1. Results of study of Pb–Pb hadron production: [14] in the heading: the total quadratic relative error $\chi^2_{\rm T}$, number of data points N, parameters p and redundancies r; in the upper section: statistical model parameters which best describe the experimental results for Pb–Pb data. Bottom section: specific energy, entropy, anti-strangeness, net strangeness of the full hadron phase space characterized by these statistical parameters. In column one, all statistical parameters and the flow vary. In column two, we fix λ_s by requirement of strangeness conservation, and in column three, we fix γ_q at the pion condensation point $\gamma_q = \gamma_q^c$.

	$\mathrm{Pb}\vert_v$	$\mathrm{Pb}\vert_v^{\rm sb}$	$\mathrm{Pb}\vert_v^{\rm sc}$
$\chi^2_{\rm T};\ N;p;r$	$2.5;\ 12;6;2$	$3.2;\ 12;5;2$	$2.6;\ 12;5;2$
T_f [MeV]	142 ± 3	144 ± 2	142 ± 2
v_c	0.54 ± 0.04	0.54 ± 0.025	0.54 ± 0.025
λ_q	1.61 ± 0.02	1.605 ± 0.025	1.615 ± 0.025
λ_s	1.09 ± 0.02	1.10^*	1.09 ± 0.02
γ_q	1.7 ± 0.5	1.8 ± 0.2	$\gamma_q^{c*} = e^{m_\pi/2T_f}$
γ_s/γ_q	0.79 ± 0.05	0.80 ± 0.05	0.79 ± 0.05
E_f/B	7.8 ± 0.5	7.7 ± 0.5	7.8 ± 0.5
S_f/B	42 ± 3	41 ± 3	43 ± 3
s_f/B	0.69 ± 0.04	0.67 ± 0.05	0.70 ± 0.05
$(\bar{s}_f - s_f)/B$	0.03 ± 0.04	0^*	0.04 ± 0.05

the chemical freeze-out is due to the direct fireball breakup.

More generally, the chemical analysis evidence for the QGP nature of the fireball is as follows: [14]

a) The value of strange quark fugacity λ_s we find in our analysis can also be obtained from the requirement that strangeness balances, $\langle N_s - N_{\bar{s}} \rangle = 0$, in QGP, which for a source in which all s an $\bar{s}$ quarks are unbound and thus have symmetric phase space, implies $\lambda_s = 1$. However, the Coulomb distortion of the strange quark phase space plays an important role in the understanding of this constraint for Pb–Pb collisions, citeRaf91 leading to the Coulomb-deformed value $\lambda_s \simeq 1.1$, which is identical to the value obtained from experimental data analysis $\lambda_s^a = 1.09 \pm 0.02$.

b) The phase space occupancy of light quarks γ_q even if it were before gluon fragmentation near or at the equilibrium value $\gamma_q = 1$, must increase above this equilibrium value. There is an upper limit: $\gamma_q < \gamma_q^c \equiv e^{m_\pi/2T_f} \simeq 1.67$, which arises to maximize the entropy density in the confined hadron phase. In our analysis we find values in this narrow interval $1 \leq \gamma_q \leq \gamma_q^c$

c) The strange quark phase space occupancy γ_s we compute within the framework of kinetic theory where strangeness pair production arises in gluon fu-

sion, [9]. The result depends on temperature reached in early stages of the collision, and following dilution effect in which the already produced strangeness can even over saturate the 'thiner' low temperature phase space. Moreover, some gluon fragmentation also enriches γ_s as measured by hadron abundance, and thus we find $gmma_s \geq 1$. We note that the ratio γ_s/γ_q has been earlier confounded with γ_s, which therefore is stated in table 1.
d) The strangeness yield, $N_s/B = N_{\bar{s}}/B \simeq 0.7$, predicted early on as the result of QGP formation [9] is also one of the results of data analysis seen in table 1. This result we obtain within the modern kinetic model of strangeness production in QGP. [14] The results are shown in figure 4 as function of the intrinsic specific energy available in the fireball E/B, for the three collision systems S-Au/W/Pb (short-dashed line), Ag–Ag (long dashed) and Pb–Pb (solid line). The solid square is the 'experimental' result obtained in our analysis of the S-Au/W/Pb system, and the open square is for Pb–Pb. The experimental value of stopping we employ (see legend to figure 4) were obtained by NA49 collaboration, [29].

Stopping enters the computation of the initial temperature from the collision energy, see Eq. (6). We extrapolate as function of E/B, assuming that the stopping fraction for the collisional pressure is known, and as here assumed, not changing with collision energy in the narrow interval shown in figure 4, leading to a steep rise of strangeness production with collision energy.

4 Supercooling and sudden breakup

4.1 Instability condition

Sudden hadronization of dense matter fireballs formed in 158A GeV Pb–Pb collisions requires that a global instability of the dense hadronic matter fireball is encountered in its evolution. Given the hadronization temperature we found, $T \simeq 143\,\mathrm{MeV}$, which is about 15 MeV below the equilibrium phase transition of QGP phase to hadron gas it is a natural step to consider the possibility of supercooling of the QGP phase. As many of us have experienced in diverse daily life experiences, once the supercooled phase is disturbed, a truly sudden break-up occurs. QGP instability was suggested by Csörgő and Csernai [28] to explain sudden hadronization. [30] Despite extensive ensuing study of potential microscopic mechanisms, [31,32,33] a convincing elementary instability mechanism has not been found.

As the fireball expands, energy is transfered from thermal motion to collective flow in adiabatic fashion. At a certain point in deep supercooling, energy flow is reversed, and the matter flow begins to slow down. However, if

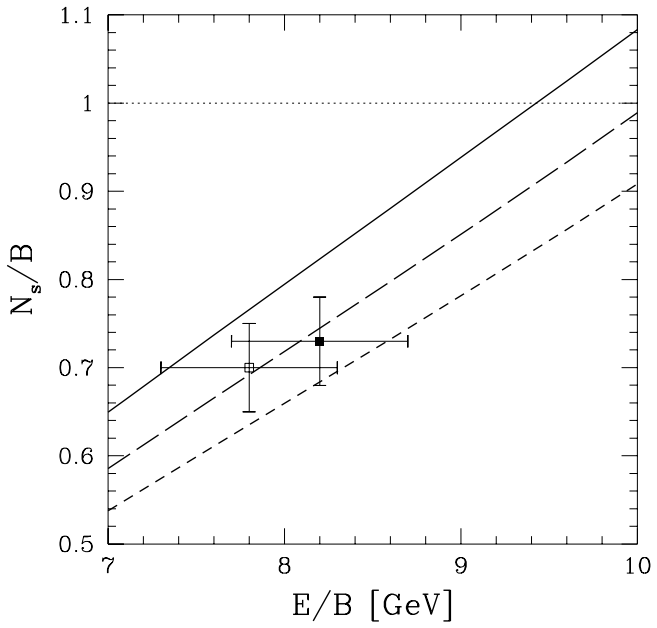

Figure 4. QGP fireball specific per baryon strangeness abundance as function of E/B energy per baryon in the fireball, for running $\alpha_{\rm s}(M_Z) = 0.118$ and $m_{\rm s}(1GeV) = 200\,{\rm MeV}$, corresponding to $m_{\rm s}(M_Z) = 90\,{\rm MeV}$. Solid lines: for Pb–Pb, stopping 57% and 360 participants, long-dashed lines: for Ag–Ag, stopping 54% and 180 participants, short-dashed lines: for S–Au/W/Pb stopping 52% and 90 participants in QGP fireball. The solid square is the result of an analysis for S-Au/W/Pb 200A GeV reaction system, and open square for Pb–Pb at 158A GeV, as shown in the lower section of table 1.

the flow velocity remains large but the surface pressure $\mathcal{P} \to 0$, continued expansion must rip the fireball apart. This is the natural mechanical instability we proposed as the sudden hadronization condition. [16] This simple mechanism does not require a microscopic process for the onset of instability.

We consider the exploding fireball dynamics in its center of momentum frame of reference. The surface normal vector of exploding fireball is $\vec{n}$, and the local velocity of matter flow $\vec{v}_{\rm c}$. The rate of momentum flow vector $\vec{\mathcal{P}}$ at the surface is obtained from the energy-stress tensor T_{kl}: [34]

$$\vec{\mathcal{P}} = P^{(i)}\vec{n} + (P^{(i)} + \varepsilon^{(i)})\frac{\vec{v}_{\rm c}\,\vec{v}_{\rm c}\cdot\vec{n}}{1-\vec{v}_{\rm c}^{\,2}}\,. \tag{7}$$

The upper index (i) refers for the intrinsic energy density ε and pressure P of matter in the frame of reference, locally at rest, *i.e.,* observed by a comoving observer. We omit the superscript (i) in the following. For the fireball expansion to continue, $\mathcal{P} \equiv |\vec{\mathcal{P}}| > 0$ is required. For $\mathcal{P} \to 0$ at $v_{\rm c} \neq 0$, we have a conflict between the desire of the motion to stop or even reverse, and the continued inertial expansion.

When the flow velocity remains large but $\mathcal{P} \to 0$, the intrinsic pressure P must be negative. As illustration consider the fireball to be made of a quark-gluon liquid confined by an external vacuum pressure $\mathcal{B}$. The total pressure and energy comprise particle (subscript $_{\rm p}$) and the vacuum properties:

$$P = P_{\rm p} - \mathcal{B}\,, \quad \varepsilon = \varepsilon_{\rm p} + \mathcal{B}\,. \tag{8}$$

Eq. (7) with $\vec{\mathcal{P}} = 0$ thus reads:

$$\mathcal{B}\vec{n} = P_{\rm p}\vec{n} + (P_{\rm p} + \varepsilon_{\rm p})\frac{\vec{v}_{\rm c}\,\vec{v}_{\rm c}\cdot\vec{n}}{1 - v_{\rm c}^2}\,, \tag{9}$$

and it describes the (equilibrium) condition where the pressure of the expanding quark-gluon fluid is just balanced by the external vacuum pressure.

Expansion beyond $\mathcal{P} \to 0$ is in general not possible. A surface region of the fireball that reached it but continues to flow outwards must be torn apart. This is a collective instability and thus the ensuing disintegration of the fireball matter will be very rapid, provided that much of the surface reaches this condition. We adopt the condition $\vec{\mathcal{P}} = 0$ at any surface region to be the instability condition of an expanding hadron matter fireball.

Negative internal pressure $P < 0$ is a requirement. At this stage the fireball must thus be significantly supercooled. The adiabatic transfer of internal heat into accelerating flow of matter provides the mechanism which leads on the scale of $\tau = 2\,10^{-23}\,$s to the development of this 'deep' supercooling.

4.2 Consistency with QGP properties

The sudden break up due to mechanical instability of course will occur for all phases of elementary matter and thus we consider next in how far the observed freeze-out conditions and other features of hadronization process are consistent with the QGP mechanical breakup, and explore if experiments show evidence for supercooling.

It is possible to determine experimentally if the condition $P < 0$ has been reached. Namely, the Gibbs-Duham relation for a unit volume:

$$P = T\sigma + \mu_{\rm b}\nu_{\rm b} - \varepsilon\,, \tag{10}$$

relates the pressure, to entropy density $\sigma = S/V$, energy density $\varepsilon = E/V$, and baryon density $\nu_{\rm b} = b/V$, V is the volume, T is the temperature, and $\mu_{\rm b}$ the baryochemical potential. Dividing by ε we obtain:

$$\frac{PV}{E} = \frac{T_{\rm h}}{E/S} + \frac{\mu_{\rm b}}{E/B} - 1\,. \tag{11}$$

The microscopic processes governing the fireball breakup determine how the quantities entering the right hand side of Eq. (11) are changed as hadrons emerge. Understanding this we can determine, if the intrinsic fireball pressure prior to breakup, has been negative.

The energy E and baryon content b of the fireball are conserved. Entropy S is conserved when the gluon content of a QGP fireball is transformed into quark pairs in the entropy conserving process $G+G \to q+\bar{q}$. Similarly, when quarks and antiquarks recombine into hadrons, entropy is conserved in the range of parameters of interest here. Thus also E/B and S/B is conserved across hadronization condition. The sudden hadronization process also maintains the temperature T and baryo-chemical potential μ_b across the phase boundary. What changes in QGP breakup are the chemical occupancy parameters. As gluons convert into quark pairs and hadrons $\gamma_g \to 0$ but the number occupancy of light valance quark pairs increases $\gamma_q > \gamma_{q_0} \simeq 1$ increases significantly, along with the number occupancy of strange quark pairs $\gamma_s > \gamma_{s_0} \simeq 1$.

Evaluating Eq. (11) using the results of the data analysis presented above, we indeed obtain $P_f < 0$. The magnitude of $|P_f|$ can vary between a few percent (in terms of energy density E_f/V), up to 20% for the latest published result. [14] The precise value, which arises from several cancellations of larger numbers is sensitive to the strategy of how the currently available experimental data is described, *e.g.,* if strangeness conservation is implemented, and if so, if differentially at each rapidity, or as an overall conservation law; how many high mass resonances can be excited in hadronization process, etc ...

Understanding in detail the breakup condition $\mathcal{P} \to 0$ requires that we model the shape and direction of flow in the late stage of fireball evolution, obviously not an easy task. However, considering $\vec{n}\cdot\vec{\mathcal{P}} \to 0$, we find the constraint:

$$\frac{-PV/E}{1+PV/E} = \kappa\frac{v_{\rm c}^2}{1-v_{\rm c}^2}\,, \quad \kappa = (\vec{v}_{\rm c}\cdot\vec{n})^2/v_{\rm c}^2\,. \tag{12}$$

For an exactly symmetrical, spherical expansion the two vectors $\vec{v}_{\rm c}$ and $\vec{n}$ are everywhere parallel, thus $\kappa \to 1$. However, in 158A GeV Pb–Pb reactions the longitudinal flow is considerably greater than the transverse flow, [29] and we

note $\kappa \to 0$ for a longitudinally evolving cylindrical fireball. For the Pb–Pb collisions considered here, our analysis suggest $0.1 < \kappa < 0.6$.

We now substitute, in Eq. (12), the fireball matter properties employing the Gibbs-Duham relation, Eq. (10), and arrive at:

$$\frac{E}{S} = \left(T_{\rm h} + \frac{\mu_{\rm b}}{S/B} \right) \left\{ 1 + \kappa \frac{v_{\rm c}^2}{1 - v_{\rm c}^2} \right\} . \tag{13}$$

Eq. (13) establishes a general constraint characterizing the fireball breakup condition.

Deep supercooling requires a first order phase transition, and this in turn implies presence of latent heat $\mathcal{B}$. Physical consistency then requires presence of external (negative) vacuum pressure $-\mathcal{B}$. We now combine the theoretical properties of the QGP equations of state with the dynamical fireball properties in order to constrain $\mathcal{B}$. Reviewing Eq. (11), we obtain:

$$-\frac{PV}{E}\varepsilon_{\rm QGP} + P_{\rm p} = \mathcal{B}\,, \tag{14}$$

To evaluate $\mathcal{B}$, we note that lattice results for $\varepsilon_{\rm QGP}$ are well represented by $\varepsilon_{\rm QGP} = aT^4$, with $a \simeq 11$, value extrapolated for the number of light quark flavors being $n_f = 2.5$ at the hadronization point. [15] We obtain, for the fireball formed in Pb–Pb reactions,

$$0.2 \cdot 11 T_{\rm h}^4 \simeq 0.17 \text{ GeV/fm}^3 \leq \mathcal{B}\,.$$

5 Thermal freeze-out

5.1 Direct and decay $m_\perp$-spectra

We next study the shape of hadron $m_\perp$-spectra. These are strongly influenced by resonance decays, which have also contributed in an important fashion to the yield of all stable hadrons observed.

The final particle distribution is composed of directly produced particles and decay products of heavier hadronic resonances:

$$\frac{dN_X}{dm_\perp} = \left.\frac{dN_X}{dm_\perp}\right|_{\rm direct} + \sum_{\forall R \to X+2+\cdots} \left.\frac{dN_X}{dm_\perp}\right|_{R \to X+2+\cdots} \tag{15}$$

Here, $R(M, M_T, Y) \to X(m, m_T, y) + 2(m_2) + \cdots$, where we indicate by the arguments that only for the decay particle X we keep the information about the shape of the momentum spectrum.

In detail, the decay contribution to yield of X is:

$$\frac{dN_X}{dm_\perp^2\,dy} = \frac{g_r b}{4\pi p^*}\int_{Y_-}^{Y_+} dY \int_{M_{T_-}}^{M_{T_+}} dM_T^2\, J\, \frac{d^2N_R}{dM_T^2 dY} \tag{16}$$

$$J = \frac{M}{\sqrt{P_T^2 p_T^2 - \{ME^* - M_T m_T \cosh\Delta Y\}^2}}$$

We have used $\Delta Y = Y - y$, and $\sqrt{s}$ is the combined invariant mass of the decay products other than particle X and $E^* = (M^2 - m^2 - m_2^2)/2M$, $p^* = \sqrt{E^{*2} - m^2}$ are the energy and momentum of the decay particle X in the rest frame of its parent. The limits on the integration are the maximum values accessible to the decay product X:

$$Y_\pm = y \pm \sinh^{-1}\left(\frac{p^*}{m_T}\right)$$

$$M_{T_\pm} = M\frac{E^* m_T \cosh\Delta Y \pm p_T\sqrt{p^{*2} - m_T^2\sinh^2\Delta Y}}{m_T^2\sinh^2\Delta Y + m^2}$$

The theoretical primary particle spectra (both those directly produced and parents of decay products) are derived from the Boltzmann distribution by Lorenz-transforming from a flowing intrinsic fluid element to the CM-frame, and integrating over allowed angles between particle direction and local flow.

We introduce in the current analysis two velocities: a local flow velocity v of fireball matter where from particles emerge, and hadronization surface (breakup) velocity which we refer to as $v_f^{-1} \equiv dt_f/dx_f$. Particle production is controlled by the effective volume element, which comprises this quantity. In detail:

$$dS_\mu p^\mu = d\omega\left(1 - \frac{\vec{v}_f^{-1}\cdot\vec{p}}{E}\right), \qquad d\omega \equiv \frac{d^3x d^3p}{(2\pi)^3}\,. \tag{17}$$

The Boltzmann distribution we adapt has thus the form

$$\frac{d^2N}{dm_T dy} \propto \left(1 - \frac{\vec{v}_f^{-1}\cdot\vec{p}}{E}\right)\gamma\, m_T\cosh y\, e^{-\gamma\frac{E}{T}\left(1-\frac{\vec{v}\cdot\vec{p}}{E}\right)}, \tag{18}$$

where $\gamma = 1/\sqrt{1-v^2}$.

The normalization for each hadron type $h = X, R$ is

$$N^h = V_{\rm QGP}\prod_{i\in h}^{n}\lambda_i\gamma_i\,.$$

We use the chemical parameters λ_i, γ_i $i = q, s$ which are as defined in [14] and commonly used to characterize relative and absolute abundances of light and strange quarks.

The best thermal and chemical parameters which minimize the total relative error $\chi^2_{\rm T}$,

$$\chi^2_{\rm T} = \sum_i \left(\frac{F_i^{\rm theory} - F_i}{\Delta F_i} \right)^2 ,$$

for all experimental measurement points F_i having measurement error ΔF_i are determined by considering simultaneously all strange baryon and antibaryon results of experiment WA97, [18] *i.e.,* Λ, $\overline{\Lambda}$, Ξ, $\overline{\Xi}$, $\Omega + \overline{\Omega}$, as well as K^0_S, except that we assign additional systematic error to these data (see below).

5.2 Λ-, $\overline{\Lambda}$-, Ξ-, $\overline{\Xi}$-$m_\perp$-*spectra*

In recent months experiment WA97 determined the absolute normalization of the published $m_\perp$ distribution, [18] and we took the opportunity to perform the shape analysis together with yield analysis in order to check if the thermal and chemical freeze-out conditions are the same. [17] Our analysis addresses the data differentiated in four different collision centralities. This allows to study the effect of the changing volume within the limits of precision set by the current data.

Since particle spectra we consider have a good relative normalization, only one parameter is required for each centrality in order to describe the absolute normalization of all six hadron spectra. This is for two reasons important:
a) we can check if the volume from which strange hadrons are emitted grows with centrality of the collision as we expect;
b) we can determine which region in $m_\perp$ produces the excess of Ω noted in the chemical fit. [14]

However, since the normalization $V_{\rm QGP}$ common for all particles at given centrality comprises additional experimental acceptance normalization which we have not yet studied, we have not normalized the value of the fireball emission volume at each centrality. Hence we will be presenting the volume parameter as function of centrality in arbitrary units.

If thermal and chemical freeze-outs are identical, our present results must be consistent with earlier chemical analysis of hadron yields. Since the experimental data we here study is dominated by the shape of $m_\perp$-spectra and not by relative particle yields, our analysis is de facto comparing thermal and chemical freeze-outs.

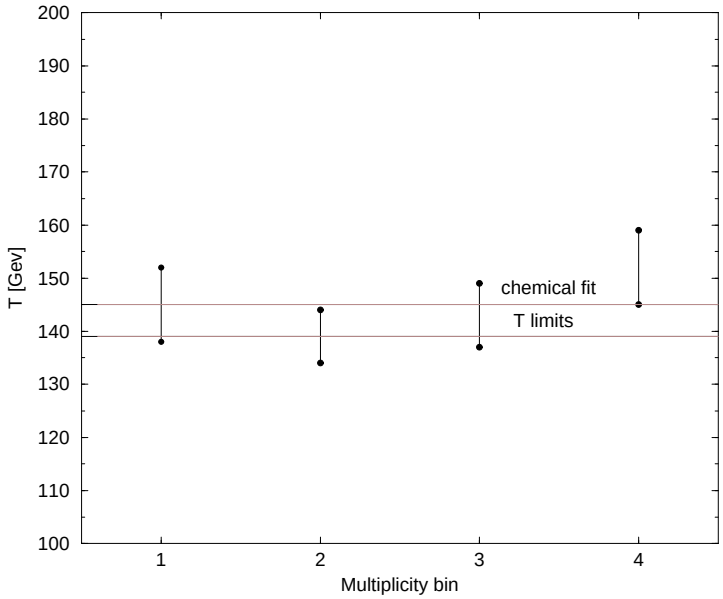

Figure 5. Thermal freeze-out temperature T for different centrality bins compared to the chemical freeze-out analysis.

We next show the parameters determining the shape of the $m_\perp$ distributions, that is T, v, v_f. As function of the centrality bin 1, 2, 3, 4 with the most central bin being 4 we show in figure 5 the freeze-out temperature T of the $m_\perp$ spectra. The horizontal lines delineate range of result of the chemical analysis. It is reassuring that we find a result consistent with the purely chemical analysis of data that included non-strange hadrons. [14] There is no indication of a significant or systematic change of T with centrality though there is a somewhat higher value in the most central 4th bin. This is consistent with the believe that the formation of the new state of matter at CERN is occurring in all centrality bins explored by the experiment WA97. Only most peripheral interactions produce a change in the pattern of strange hadron production. [35]

The (unweighted) average of all results shown in figure 5 produces a freeze-out temperature at the upper boundary of the the pure chemical freeze-out analysis result, $T \simeq 145\,\mathrm{MeV}$. It should be noted that in chemical analysis we have not distinguished between the flow v and freeze-out v_f velocity and both

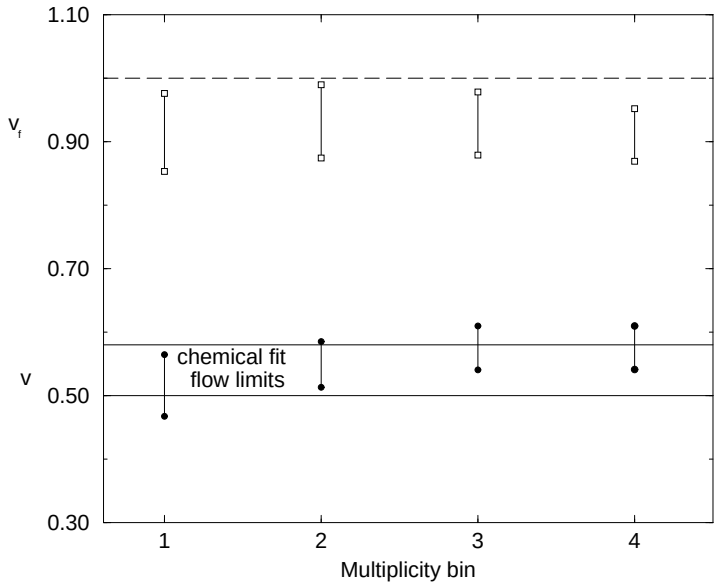

Figure 6. Thermal freeze-out flow velocity v (top) and break up (hadronization) velocity v_f for different centrality bins. Upper limit $v_f = 1$ (dashed line) and chemical freeze-out analysis limits for v (solid lines) are also shown.

are denoted as v_c, which may be the cause of this slight difference between current analysis average and the earlier purely chemical analysis result.

The magnitudes of the collective expansion velocity v and the break-up (hadronization) speed parameter v_f are presented in figure 6. For v (lower part of the figure) we again see consistency with earlier chemical freeze-out analysis results, and there is no confirmed systematic trend in the behavior of this parameter as function of centrality.

Though within the experimental error, one could argue inspecting figure 6 that there is systematic increase in transverse flow velocity v with centrality and thus size of the system. This is expected, since the more central events comprise greater volume of matter, which allows more time for development of the flow. Interestingly, it is in v and not T that we find the slight change of spectral slopes noted in the presentation of the experimental data. [18]

The value of the beak-up (hadronization) speed parameter v_f shown in

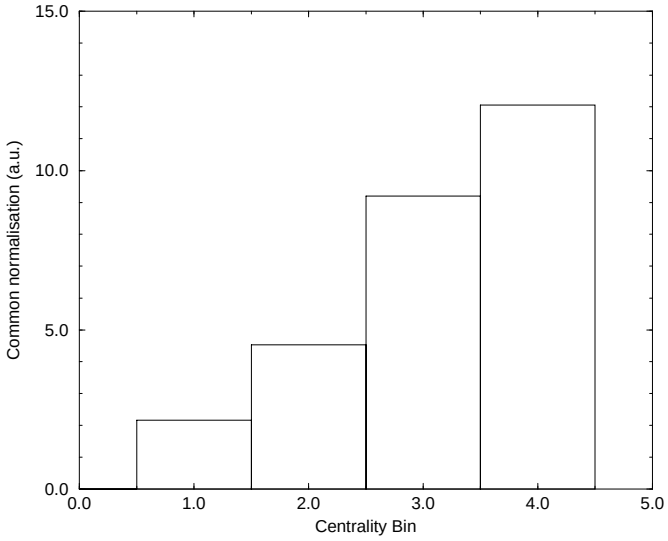

Figure 7. Hadronization volume (arbitrary units) for different centrality bins.

the top portion of figure 6 is near to velocity of light which is consistent with the picture of a sudden breakup of the fireball. This hadronization surface velocity v_f was in the earlier chemical fit set to be equal to v, as there was not enough sensitivity in purely chemical fit to determine the value of v_f.

Unlike the temperature and two velocities, the overall normalization of hadron yields, V^h is found to be strongly centrality dependent, as is seen in figure 7. This confirms in quantitative way the believe that the entire available fireball volume is available for hadron production. The strong increase in the volume by factor six is qualitatively consistent with a geometric interpretation of the collision centrality effect. Not shown is the error propagating from the experimental data which is strongly correlated to the chemical parameters discussed next. This systematic uncertainty is another reason we do not attempt an absolute unit volume normalization.

The four chemical parameters $\lambda_q, \lambda_s, \gamma_q, \gamma_s/\gamma_q$ are shown in the following figures 8, 9. These parameters determine along with V^h the final particle yield. Since we have 5 parameters determining normalization of 6 strange hadron spectra, and as discussed we reduce the statistical weight of Kaons, there is obviously a lot of correlation between these 4 quantities, and thus the

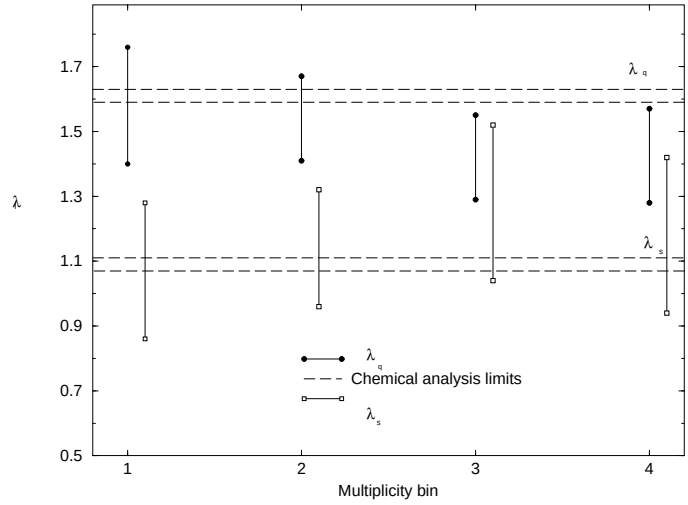

Figure 8. Thermal analysis chemical quark fugacity λ_q (top) and strange quark fugacity λ_s (bottom) for different centrality bins compared to the chemical freeze-out analysis results.

error bar which reflects this correlation, is significant.

The chemical fugacities λ_q and λ_s shown in figure 8 do not exhibit a systematic centrality dependence. This is consistent with the result we found for T in that the freeze-out properties of the fireball are seen to be for the temperature and chemical potential values independent of the size of the fireball. Comparing to the earlier chemical freeze-out result in figure 8 one may argue that there is a systematic downward deviation in λ_q. However, this could be caused by the fact that the chemical freeze-out analysis allowed for isospin-asymmetric $\Xi^-(dss)$ yield, [14] while out present analysis is not yet distinguishing light quarks.

The ratio γ_s/γ_q shown in bottom portion of figure 9 is systematically smaller than unity, consistent with many years of prior analysis: when $\gamma_q = 1$ is tacitly chosen, this ratio is the value of γ_s in analysis of strange baryons. We have not imposed a constrain on the range of γ_q (top of figure 9) and thus values greater than the pion condensation point $\gamma_q^* = e^{m_\pi/2T} \simeq 1.65$ (thick line) can be expected, but in fact do not arise.

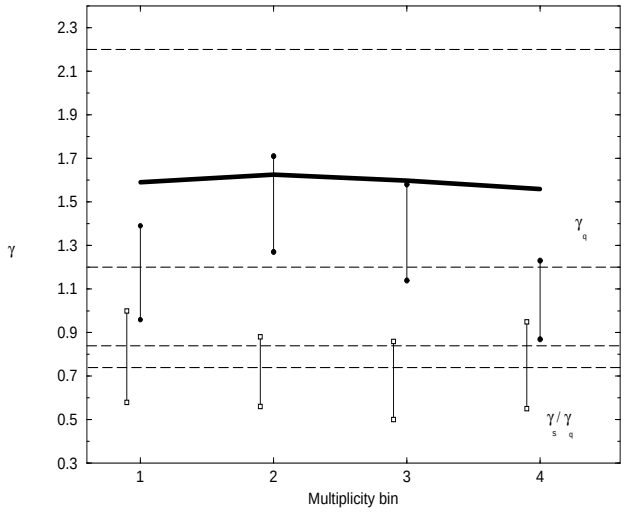

Figure 9. Thermal analysis chemical quark abundance parameter γ_q (top) and γ_s/γ_q (bottom) for different centrality bins compared to the chemical freeze-out analysis. Thick line: upper limit arising with pion condensation.

It is important to explicitly check how well the particle $m_\perp$-spectra are reproduced. We group all bins in one figure and show in figures 10, 11, 12, 13 in sequence Λ, $\overline{\Lambda}$, Ξ, $\overline{\Xi}$. Overall, the description of the shape of the spectra is very satisfactory.

5.3 Omega and Meson spectra

In figure 14 all four centrality bins for the sum $\Omega + \overline{\Omega}$ are shown. We see that we systematically under predict the two lowest $m_\perp$ data points. Some deviation at high $m_\perp$ may be attributable to acceptance uncertainties, also seen in the the Ξ result presented earlier in figure 13. We recall that there is a disagreement between theoritical expectation and the Omega yields. In the here presented thermal analysis, we see that this disagreement is arising at low momentum. We could include all experimental results in the present analysis since the omega data have a relative low statistical evidence and thus other hyperon data determine the behavior of Ω-spectrum.

The low-$m_\perp$ anomaly also explains why the inverse $m_\perp$ slopes for Ω, $\overline{\Omega}$ are smaller than the values seen in all other strange (anti)hyperons. One can presently only speculate about the processes which contribute to this anomaly.

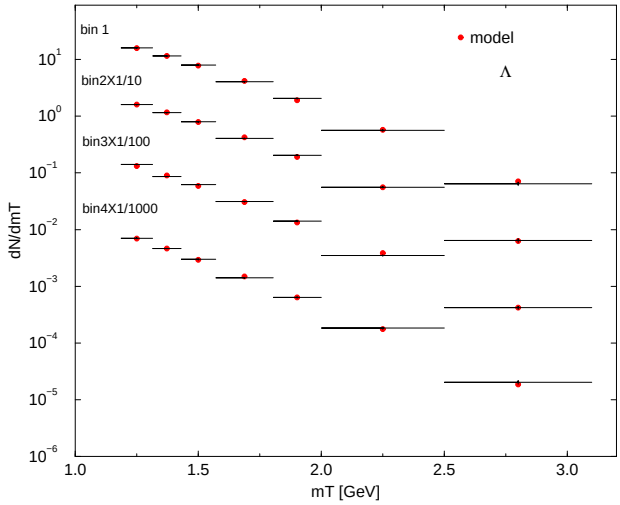

Figure 10. Thermal analysis m_T spectra: Λ

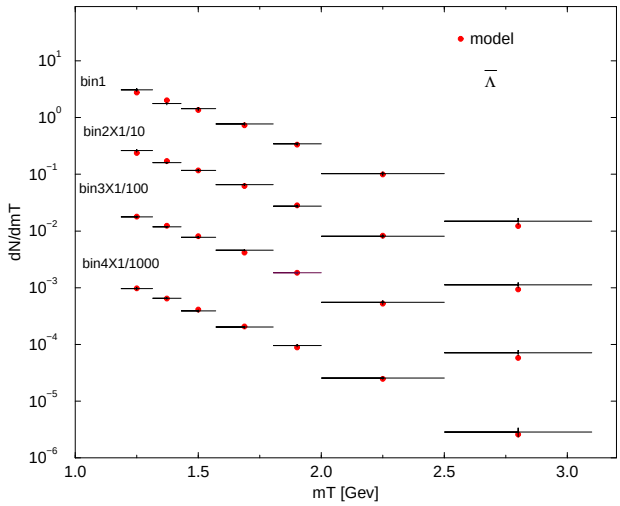

Figure 11. Thermal analysis m_T spectra: $\overline{\Lambda}$.

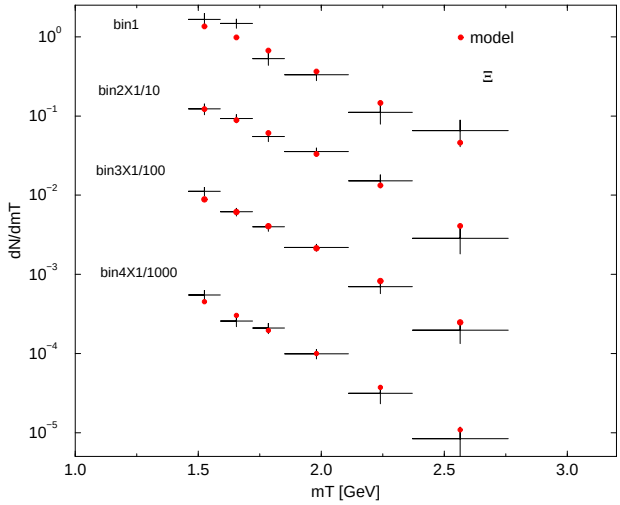

Figure 12. Thermal analysis m_T spectra: Ξ

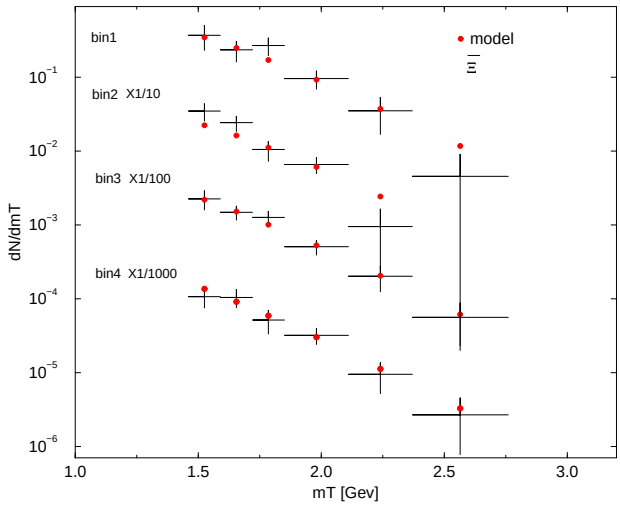

Figure 13. Thermal analysis m_T spectra: $\overline{\Xi}$

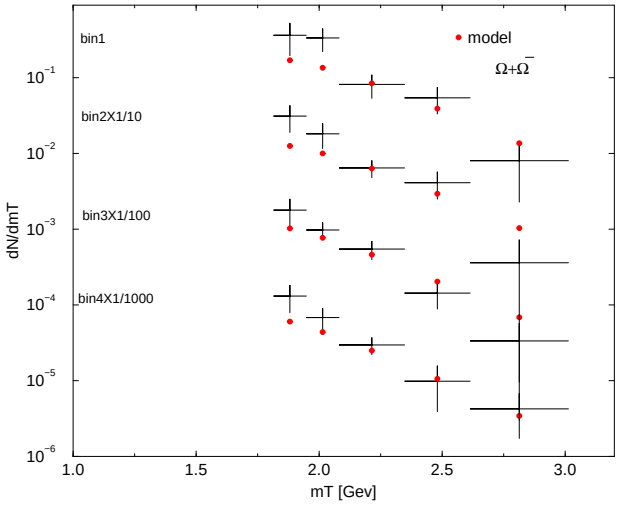

Figure 14. Thermal analysis m_T spectra: $\Omega + \overline{\Omega}$.

We note that the 1–2s.d. deviations in the low $m_\perp$-bins of the $\Omega+\overline{\Omega}$ spectrum translates into 3s.d. deviations from the prediction of the chemical analysis. This is mainly a consequence of the fact that after summing over centrality and $m_\perp$, the statistical error which dominates $\Omega+\overline{\Omega}$ spectra becomes relatively small, and as can be seen the low $m_\perp$ excess practically doubles the yield.

For kaons K^0 the statistical errors are very small, and we find in a more in depth statistical analysis that they must be smaller than the systematic errors not considered. This is done checking the influence of the deletion of individual measurement points in the spectrum on the fit result, which influences the outcome in case of kaons only. We assign in a somewhat arbitrary manner a systematic error that we arbitrarily choose to be 5 times greater than statistical error.

With this modification we included the kaon data in the analysis which included the above presented strange baryon and antibaryon results. Because of the large error we assigned, there is relatively little influence the kaon spectra have on the baryon/antibaryon analysis. In fact the kaon results show how the hyperon/antihyperon experimental results predict K^0_S-$m_\perp$ spectra. We describe the kaon data well, and especially so in the $m_\perp$ range which is the same as that for hyperons considered earlier, as is seen in figure 15.

We now turn to the pion spectra measured by the WA98 collaboration. [36]

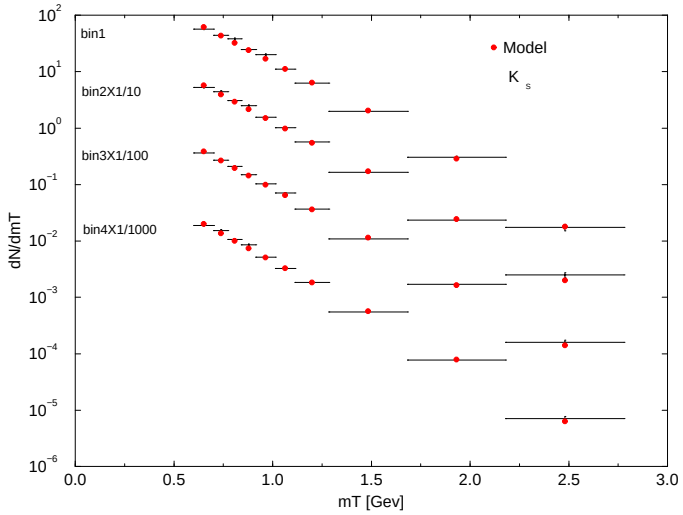

Figure 15. Thermal analysis m_T spectra: K_s.

This is a very difficult matter, since at low momenta there are many mechanisms of pion production which we have not analyzed. Moreover, we have not fully understood how the longitudinal flow influences through the secondary decays the observed pion spectra. Compared to strange hadrons we study the π^0 data in a very wide range of $m_\perp$ in which the yield changes by 6 orders of magnitude.

We use a set of parameters obtained fro the hyperon data, *i.e.,* $T_f = 143\,\mathrm{MeV}$, setting also freeze-out surface velocity $0.99c$. We include in the results shown in figure 16 aside of directly produced pions the two body decay of the ρ. We allow a direct hard parton QCD component contribution, [38] of the form

$$Ed^3N/d^3p \propto 1/p_\perp^\kappa \,.$$

Thus, we vary four parameters: two normalizations (thermal and QCD direct component), and also $\kappa = 5.6 \pm 1.2$, $v_c = 0.55 \pm 0.02$, with resulting best fits as stated. This procedure yields a good description of the data as seen in figure 16, with $\chi^2/\mathrm{dof} < 1.4$. Considering that only statistical error is being considered, and we were not evaluating contributions of 3-body decay resonances, we see this as a noteworthy confirmation that the hard pions are also created primarily in the sudden hadronization process. We note that the

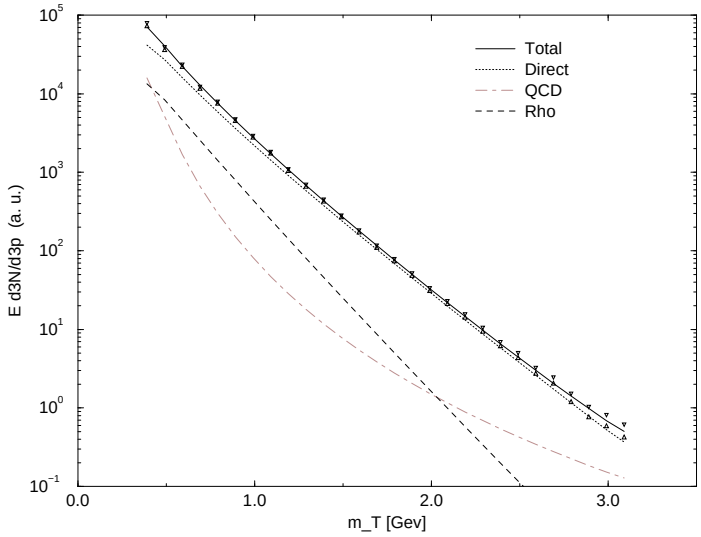

Figure 16. Central rapidity data of experiment WA98 for π^0 are compared to the spectra expected in a sudden freeze-out reaction picture. See text for details.

direct QCD component is at 1–20% level, and thus before proceeding further a more precise model of this contribution needs to be developed.

Our analysis is not contradicting results shown in [36], for these authors did not consider that the freeze-out surface velocity is different from the flow velocity, and they did not allow for direct parton-parton scattering contributions in their analysis of pion spectra.

Our results confirm the finding that the apparent temperature hierarchy for different mass particles is due to a collective expansion of the source. [37]

6 Strangeness at RHIC

6.1 Expectations

The abundances of particles produced from QGP within the sudden freeze-out model are controlled by several parameters we restate here: the light quark fugacity $1 < \lambda_q < 1.1$, value is limited by the expected small ratio between baryons and mesons (baryon-poor plasma) when the energy per baryon is above 100 GeV, strangeness fugacity $\lambda_s \simeq 1$ which value for locally neutral plasma assures that $\langle s - \bar{s} \rangle = 0$; the light quark phase space occupancy $\gamma_q \simeq$

Table 2. For $\gamma_s = 1.25$, $\lambda_s = 1$ and γ_q, λ_q as shown: Top portion: strangeness per baryon s/B, energy per baryon E/B[GeV] and entropy per baryon S/B. Bottom portion: sample of hadron ratios expected at RHIC.

γ_q	1.25	1.5	1.5	1.5	1.60
λ_q	1.03	1.025	1.03	1.035	1.03
E/B[GeV]	117	133	111	95	110
s/B	18	16	13	12	12
S/B	630	698	583	501	571
$p/\bar{p}$	1.19	1.15	1.19	1.22	1.19
Λ/p	1.74	1.47	1.47	1.45	1.35
$\bar{\Lambda}/\bar{p}$	1.85	1.54	1.55	1.55	1.44
$\bar{\Lambda}/\Lambda$	0.89	0.91	0.89	0.87	0.89
Ξ^-/Λ	0.19	0.16	0.16	0.16	0.15
$\overline{\Xi^-}/\bar{\Lambda}$	0.20	0.17	0.17	0.17	0.16
$\overline{\Xi}/\Xi$	0.94	0.95	0.94	0.93	0.94
Ω/Ξ^-	0.147	0.123	0.122	0.122	0.115
$\overline{\Omega}/\overline{\Xi^-}$	0.156	0.130	0.130	0.131	0.122
$\overline{\Omega}/\Omega$	1	1.	1.	1.	1.
$\frac{\Omega+\overline{\Omega}}{\Xi^-+\overline{\Xi^-}}$	0.15	0.13	0.13	0.13	0.12
$\frac{\Xi^-+\overline{\Xi^-}}{\Lambda+\bar{\Lambda}}$	0.19	0.16	0.16	0.16	0.15
K^+/K^-	1.05	1.04	1.05	1.06	1.05

1.5, overabundance value due to gluon fragmentation. Given these narrow ranges of chemical parameters and the sudden freeze-out temperature $T_f = 150$ MeV expected for nearly baryon free domain, we compute the particle production at break-up.

Taking $\gamma_q = 1.5^{+0.10}_{-0.25}$, we choose the value of λ_q, see the header of table 2, for which the energy per baryon (E/B) is similar to the collision condition (100 GeV), which leads to the range $\lambda_q = 1.03 \pm 0.005$. We evaluate for these examples aside of E/B, the strangeness per baryon s/B and entropy per baryon S/B as shown in the top section of the table 2. We do not enforce $\langle s - \bar{s} \rangle = 0$ at central rapidity exactly, but since baryon asymmetry is small, strangeness is balanced to better than 2% in the parameter range considered. In the bottom portion of table 2, we present the compatible particle abundance ratios, computed according to the procedure we developed, and described above. [14] We have given, aside of the baryon and antibaryon relative yields, also the relative kaon yield, which is also well determined within this approach.

The meaning of these results can be better appreciated when we assume in an example the central rapidity density of direct protons is $dp/dy|_{\rm cent.} = 25$.

Table 3. $dN/dy|_{\rm cent.}$ assuming in this example $dp/dy|_{\rm cent.} = 25$.

γ_q	λ_q	b	p	$\bar{p}$	$\Lambda{+}\Sigma^0$	$\overline{\Lambda}{+}\overline{\Sigma}^0$	$\Sigma^\pm$	$\overline{\Sigma}^\mp$	Ξ^0	$\overline{\Xi}^0$	$\Omega{=}\overline{\Omega}$
1.25	1.03	17	25*	21	44	39	31	27	17	16	1.2
1.5	1.025	13	25*	22	36	33	26	23	13	11	0.7
1.5	1.03	16	25*	21	37	33	26	23	12	11	0.7
1.5	1.035	18	25*	21	36	32	26	22	11	10	0.7
1.60	1.03	15	25*	21	34	30	24	21	10	9.6	0.6

In table 3, we present the resulting (anti)baryon abundances. The net baryon density $db/dy \simeq 16 \pm 3$, there is baryon number transparency. We see that (anti)hyperons are indeed more abundant than non-strange (anti)baryons. Taking into account the disintegration of strange baryons, we are finding a much greater number of observed protons $dp/dy|^{\rm obs.}_{\rm cent.} \simeq 65 \pm 5$ in the central rapidity region. It is important when quoting results from table 3 to recall that:

1) we have chosen arbitrarily the overall normalization in table 3 , only particle ratios were computed, and

2) the rapidity baryon density relation to rapidity proton density is a consequence of the assumed value of λ_q, which we chose to get $E/B \simeq 100\,{\rm GeV}$ per participant.

6.2 Comparison of theory and experiment

Our study of RHIC results has just begun and we expect that it remains an ongoing project as we enter the period of RHIC data collection and analysis. Some of our predictions can already be compared with experiment (STAR at RHIC). These results are in agreement with our model of how QGP evolves at RHIC.

In order to compare with experiment, we need to adjust from the assumed 100+100A GeV RHIC energy to the RHIC run energy in 2000 which is 65+65A GeV. We consider the $\overline{\Lambda}/\Lambda$ ratio. At 8.6+8.6A GeV (corresponding to 160A GeV the experimental result is $\overline{\Lambda}/\Lambda \simeq 0.12$ while at 100+100A GeV we predict $\overline{\Lambda}/\Lambda = 0.89 \pm 0.02$ in table 2. We also made a prediction for 35+35A GeV [21], where we found $\overline{\Lambda}/\Lambda \simeq 0.5$. The interpolated result for the 65+65A GeV RHIC run is $\overline{\Lambda}/\Lambda \simeq 0.68 \pm 0.05$, which is nearly exactly the October 2000 APS-meeting STAR ratio $\overline{\Lambda}/\Lambda = 0.7 \pm 0.05 \pm 0.2$. From our

$\overline{\Lambda}/\Lambda$ ratio one obtains

$$\frac{\bar{p}}{p} = \frac{\lambda_s^2}{\lambda_q^2}\frac{\overline{\Lambda}}{\Lambda},$$

and this implies taking note of the heading and caption in table 2 that the $\bar{p}/p$ ratio is about 7% smaller compared to $\overline{\Lambda}/\Lambda$ ratio. In fact STAR reported $\bar{p}/p = 0.65 \pm 0.05$, in agreement with our result.

Both particle ratios can thus be well described within our understanding of the hadronization and properties of QGP at RHIC. In their absolute values reflect on the expected small baryon content at the initial RHIC energy. Both should increase by 25–30% at the top RHIC energy (100+100 AGeV).

The most interesting result seen in table 3 , which confirmation we anticipate and await with anxiety is the hyperon-dominance of the baryon yields at RHIC, a fact which as we believe does not depend on a detailed model hypothesis. Another interesting property of the hadronizing hot RHIC matter, as seen in table 2, is that strangeness yield per participant is expected to be 13–23 times greater than seen at present in Pb–Pb interactions at SPS energies, where we have 0.75 strange quark pairs per baryon.

7 Summary and conclusions

The enhanced strangeness yield observed at 158–200A GeV reactions corresponds according to our study to $\mathcal{O}(0.75)$ $s\bar{s}$-pairs of quarks per participant baryon, see section 3. Considering the properties of QGP-liquid explored in section 2 and the resulting initial gluon temperatures we have shown that this exceptionally high yield is achievable in a short time that the collision is known to last by in-plasma gluon-fusion reactions, $G + G \rightarrow s + \bar{s}$, as was proposed many years ago. [9]

Beyond strangeness enhancement, multi strange baryons and antibaryons have been recognized as being even a more specific source of information about the deconfined state of the matter. The analysis of experimental results from 158AGeV Pb–Pb interactions carried out in sections 3 (chemical abundance analysis) and in section 5 (spectral $m_\perp$ shape) confirms this. We find that strange baryons and antibaryons are dominantly produced in sudden hadronization of the quark-gluon fireball with chemical and thermal decoupling occurring at the same time.

From the appearance of first results we recognized that sudden hadronization is required. [30] However, initially the mechanisms leading to direct hadronization (hadron production from QGP fireball without equal rescattering), have not been theoretically understood. Here, we have presented

in section 4 a complete reaction picture consistent with QGP equations of state. [16] The sudden breakup (direct hadronization) into final state particles occurs as the QGP fireball super-cools, and in this state encounters a mechanical instability, which drives the explosive disintegration. Deep supercooling requires a first order phase transition, and this in turn implies presence of a latent heat and we have estimated its magnitude in section 4.

There are several experimental facts that lead us to consider sudden QGP hadronization. The most recent point has been the results presented in section 5 which show agreement between thermal and chemical freeze-out analysis. An important experimental input is the identity of the $m_\perp$ spectra for strange baryons and antibaryons. We have been motivated initially to pursue sudden QGP hadronization by the need to use chemical nonequilibrium to describe hadron production. At first we have proposed this for the case of strange quarks, and more recently as the experimental data became more comprehensive, we also recognized the need to consider light quark chemical nonequilibrium — we described details of these developments elsewhere. [14]

The light quark pair excess is a convenient way to understand hadron multiplicity excess, which we have related to an entropy excess. [39] But is this the only good way to understand the experimental hadron production data? It is hard to check all possibilities. However, we explored (in medium) changes of hadron masses. We have found that invariably the statistical significance of the analysis decreases as we modify individual hadron properties, as long as we have been assuming chemical equilibrium of hadron abundances, and a consistent change of both mesons and baryons properties. Our extensive trial and error searches have convinced us that the only theoretical description of hadron production data that works ($\chi^2/\mathrm{dof} < 1$) requires excess of valence light quark pair abundance, irrespective of the detailed strategy of data analysis.

So how it can be that there are many people who believe that one can describe hadron production data assuming chemical equilibrium of light quarks. In fact, if we take hadronization to somehow occur in chemical equilibrium, or/and ignore the possibility of plasma formation, we find $\chi^2/\mathrm{dof} > 2.5,\ \mathrm{dof} = 10$ in our analysis, which agrees when carried out with this assumption with results of others. [40] Even though this χ^2 is without convincing physical significance, what has caused that this result has not been forgotten is that the chemical freeze-out temperature for equilibrium condition comes out to be near to the expected equilibrium phase transition condition, $T \simeq 170\,\mathrm{MeV}$, see section 2. Thus the assumption of equilibrium seems to be consistent with the properties of QGP phase. Furthermore, the study of soft pions suggests (unlike it is with hard pions or other hadrons) that the

thermal freeze-out occurs at about 120 MeV. Naturally, soft pions can be produced by more complex collective processes not considered in the conventional thermal analysis and we thus did not introduce these particles into our study, preferring to depend on the numerous other results in section 5.

Further study of details of chemical freeze-out, involving consideration of strong resonances may lead to a direct experimental differentiation of these two alternatives. We are presently considering $\Sigma^*(1385)$, [41] which if freeze-out occurs at $T = 170\,\mathrm{MeV}$ would be the dominant source of Λ considering the decay $\Sigma^*(1385) \to \Lambda + \pi$ (88%). But we are already today quite certain about the correctness of the sudden hadronization picture since:

1. the experimental strange and non-strange, hadron abundance results statistically strongly favor chemical nonequilibrium in hadronization;
2. baryons and antibaryons have the same $m_\perp$ spectra; and
3. our recent finding from the analysis of $m_\perp$ spectra described in section 5 that the thermal freeze-out temperature is the same as the chemical non-equilibrium freeze-out condition.

Our enhanced understanding of the fireball supercooling and resulting sudden breakup, as well as our study of thermal freeze-out properties has in the past year considerably strengthened our case. Not only we can now argue that the point of instability agrees with the thermal and chemical freeze-out, but also we have considered the freeze-out surface dynamics and have shown that the break-up velocity v_f is nearly velocity of light, as would be expected in a sudden breakup of a QGP fireball.

What are the possible causes of the chemical non-equilibrium? Certainly even if the breakup of the QGP-fireball is sudden we could have abundance equilibrium. In fact, the microscopic processes governing the fireball breakup determine how the physical and statistical properties of the fireball change at the breakup point. In particular as gluons convert into quark pairs and hadrons, the gluon abundance parameter $\gamma_g \to 0$ and the quark chemical occupancy parameters have to increase significantly, as we determine in data analysis. On the other hand the energy E and baryon content b of the fireball are conserved. Entropy S is conserved when the gluon content of a QGP fireball is transformed into quark pairs in the entropy conserving process $G + G \to q + \bar{q}$. Similarly, when quarks and antiquarks recombine into hadrons, entropy is conserved in the range of parameters of interest here. Thus also E/B and S/B is conserved across hadronization condition. The sudden hadronization process also maintains the temperature T and baryo-chemical potential μ_b across the phase boundary.

We have described strange hadron $m_\perp$-spectra with astounding precision in all available centrality bins. The remarkable similarity of $m_\perp$ spectra reported by the WA97 experiment is interpreted by a set of freeze out parameters, and we see that production mechanism of Λ, $\overline{\Lambda}$, and Ξ, $\overline{\Xi}$ is the same. This symmetry, including matter–antimatter production is an important cornerstone of the claim that the strange antibaryon data can only be interpreted in terms of direct particle emission from a deconfined phase. In presence of conventional hadron collision based physics, the production mechanism of antibaryons is quite different from that of baryons and a similarity of the $m_\perp$ spectra is not expected. Moreover, even if QGP is formed, but a equal phase of confined particles is present, the annihilation of antibaryons in the baryon rich medium created at CERN-SPS energy would deplete more strongly antibaryon yields, in particular so at small momenta, with the more abundant baryons remaining less influenced. This effect is not observed. [18]

Similarity of $m_\perp$-spectra does not at all imply, and one should not expect a similarity of particle rapidity spectra. As hyperon are formed at the fireball breakup, any remaining longitudinal flow present among fireball constituents will be imposed on the product particle, thus Λ-spectra containing potentially two original valence quarks are stretched in y, which $\overline{\Lambda}$-y-spectra are not, as they are made from newly formed particles. All told, one would expect that anti-hyperons can appear with a thermal rapidity distribution, but hyperons will not. But both have the same thermal-explosive collective flow controlled shape of $m_\perp$-spectra.

The only systematic disagreement we see is that the $\Omega + \overline{\Omega}$ results have a noticeable systematic low $p_\perp$ enhancement anomaly visible in two lowest $m_\perp$ bins in all centrality bins. This result shows that it is not a different temperature of freeze-out of $\Omega + \overline{\Omega}$ that leads to more enhanced yield, but a soft momentum secondary source which contributes almost equal number of soft $\Omega + \overline{\Omega}$ compared to the yield expected in view of the behavior of other strange hadrons.

We have presented here a short overview of our recent work developing further strangeness as a signature of the formation of quark-gluon plasma, and as a diagnostic tool allowing the study of its properties. The understanding of the properties of the QGP formed in CERN-SPS experiment has greatly improved in past 18 months.

Acknowledgments

Work supported in part by a grant from the U.S. Department of Energy, DE-FG03-95ER40937.

Laboratoire de Physique Théorique et Hautes Energies, LPTHE, at University Paris 6 and 7 is supported by CNRS as Unité Mixte de Recherche, UMR7589.

References

1. N. Itoh, *Prog. Theor. Phys.* **44**, 291 (1970).
2. P. Carruthers, *Collectuve Phenomena* **1**, 147 (1973).
3. F. Iachello, W.D. Langer and W.D. Lande, *Nucl. Phys.* A **219**, 612 (1974).
4. J.C. Collins and M.J. Perry, *Phys. Rev. Lett.* **34**, 1353 (1975).
5. R. Hagedorn, in Quark Matter'84, p53, K. Kajantie, ed., Springer Lecture Notes in Physics, Vol. 221 (Springer, Berlin, 1985).
6. F. Karsch, E. Laermann and A. Peikert, *Phys. Lett.* B **478**, 447 (2000).
7. J. Rafelski, "Extreme States of Nuclear Matter", p. 282 in *Future Relativistic Heavy Ion Experiments*, R. Bock and R. Stock, Eds., GSI Report 1981-6;
   J. Rafelski, and R. Hagedorn, "From Hadron Gas to Quark Matter II", p. 253 in *Statistical Mechanics of Quarks and Hadrons*, H. Satz, ed.; (North Holland, Amsterdam, 1981);
   J. Rafelski, "Hot Hadronic Matter", p. 619 in *New Flavor and Hadron Spectroscopy*, J. Tran Thanh Van, Ed., Ed. Frontières (Paris 1981);
   J. Rafelski, "Extreme states of nuclear matter". *Nucl. Physics* A **374**, 489c (1982).
8. J. Rafelski and B. Müller, *Phys. Rev. Lett* **48**, 1066 (1982); **56**, 2334E (1986);
   P. Koch, B. Müller and J. Rafelski, *Z. Phys.* A **324**, 453 (1986).
9. J. Rafelski, *Phys. Rep.* **88**, 331 (1982).
10. J. Rafelski and M. Danos, *Perspectives in High Energy Nuclear Collisions*, NBS-IR 83-2725 Monograph, U.S. Department of Commerce, National Bureau of Standards, June 1983;
    Updated version appeared in *Nuclear Matter under Extreme Conditions*, D. Heiss, Ed., Springer Lecture Notes in Physics **231**, pp. 362-455 (1985).
11. P. Koch and J. Rafelski, *Nucl. Phys.* A **444**, 678 (1985).
12. P. Koch, B. Müller and J. Rafelski, *Phys. Rep.* **142**, 167 (1986).
13. F. Antinori *et al.*, WA97 Collaboration *Nucl. Phys.* A **663**, 717 (2000);
    E. Andersen *et al.*, WA97 collaboration, *Phys. Lett.* B **433**, 209 (1998);
    E. Andersen *et al.*, WA97 collaboration, *Phys. Lett.* B **449**, 401 (1999).
14. J. Letessier and J. Rafelski, *Int. J. Mod. Phys.* E **9**, 107, (2000), and references therein.
15. S. Hamieh, J. Letessier, and J. Rafelski, *Phys. Rev.* C **62**, 064901 (2000).

16. J. Rafelski and J. Letessier, *Phys. Rev. Lett.* **85**, 4695 (2000).
17. G. Torrieri and J. Rafelski, submitted to New J. Phys., E-print hep-ph/0012102
18. F. Antinori *et al.*, WA97 Collaboration *Eur. Phys. J.* C **14**, 633, (2000), and private communication.
19. J. Rafelski and M. Danos, *Phys. Lett.* B, **192**, 432 (1987).
20. J. Rafelski and J. Letessier, *Phys. Lett.* B **469**, 12 (1999).
21. S. Bass *et al.*, *Nucl. Phys.* A **661**, 260 (2000).
22. J. Rafelski, J. Letessier and A. Tounsi, *Acta Phys. Pol.* B **27**, 1035 (1996).
23. A. Peshier, B. Kämpfer and G. Soff, *Phys. Rev.* C **61**, 45203, (2000).
24. H. Vija and M.H. Thoma, *Phys. Lett.* B **342**, 212, (1995).
25. S.A. Chin, *Phys. Lett.* B, **78**, 552, (1978).
26. J. Letessier, A. Tounsi and J. Rafelski, *Phys. Rev.* C **50**, 406 (1994); J. Rafelski, J. Letessier and A. Tounsi, *Acta Phys. Pol.* A **85**, 699 (1994).
27. R. Hagedorn and J. Rafelski *Phys. Lett.* B **97**, 136 (1980).
28. T. Csörgő, and L.P. Csernai, *Phys. Lett.* B **333**, 494 (1994).
29. H. Appelshäuser *et al.*, NA49, *Phys. Rev. Lett.* **82**, 2471 (1999).
30. J. Rafelski, *Phys. Lett.* B **262**, 333 (1991); J. Letessier and J. Rafelski, *Acta Phys. Pol.* B **30**, 153 (1999).
31. L.P. Csernai, I.N. Mishustin, *Phys. Rev. Lett.* **74**, 5005, (1995).
32. T.S. Biró, P. Lévai, J. Zimányi, *Phys. Rev.* C **59**, 1574 (1999).
33. I.N. Mishustin, *Phys. Rev. Lett.* **82**, 4779 (1999).
34. L.D. Landau and E.M. Lifschitz, "Fluid Mechanics", (Oxford 1999); S. Weinberg, "Gravitation and Cosmology", (New York, 1972).
35. S. Kabana *et al.*, NA52 collaboration, *Nucl. Phys.* A **661**, 370c (1999); S. Kabana *et al.*, NA52 collaboration, *J. Phys.* G *Nucl. Part. Phys.* **25**, 217 (1999).
36. M. Aggarwal *et al.*, WA98 Collaboration *Phys. Rev. Lett.* **83**, 926 (1999); we thank T. Petizmann for making available the data as published.
37. I.G. Bearden *et al.*, NA44 Collaboration *Phys. Rev. Lett.* 78, 2080 (1997).
38. R.D. Fields and R.P. Feynman, *Phys. Rev.* D **15**, 2590 (1977); and R.P. Feynman, R.D. Fields and G.C. Fox, *Phys. Rev.* D **18**, 3320 (1978).
39. J. Letessier, *et al.*, *Phys. Rev. Lett.* **70**, 3530 (1993); *Phys. Rev.* D **51**, 3408 (1995).
40. P. Braun-Munzinger, I. Heppe and J. Stachel, *Phys. Lett.* B **465**, 15 (1999).
41. G. Torrieri and J. Rafelski, Σ^* *as signature of freeze-out dynamics*, E-print hep-ph/01